Beamforming Techniques for NOMA-based Integrated Sensing and Communication Systems

Journal:	*IEEE Transactions on Green Communications and Networking*
Manuscript ID	TGCN-RP-A2-25-0030
Manuscript Type:	Regular Paper - Area 2: Green Wireless Communication Networks
Date Submitted by the Author:	30-Jan-2025
Complete List of Authors:	Li, Chentong; University of York School of Physics Engineering and Technology Mohammadzadeh, Saeed; University of York School of Physics Engineering and Technology Al-Obiedollah, Haitham ; The Hashemite University Faculty of Engineering Cumanan, kanapathippillai; University of York School of Physics Engineering and Technology Dobre, Octavia; Memorial University of Newfoundland Department of Electrical and Computer Engineering
Keyword:	Communication, Minimization methods, Space division multiplexing

Beamforming Techniques for NOMA-based Integrated Sensing and Communication Systems

Chentong Li, Saeed Mohammadzadeh, *Member, IEEE,*
Haitham Al-Obiedollah, *Member, IEEE,*
Kanapathippillai Cumanan, *Senior Member, IEEE,* and Octavia A. Dobre. *Fellow, IEEE*

Abstract

In this paper, beamforming techniques are proposed for an integrated sensing and communication (ISAC) system based on non-orthogonal multiple access (NOMA). Specifically, a multi-antenna dual-functional base station simultaneously performs target sensing and serves multiple single-antenna NOMA communication users. To investigate the potential capabilities of this NOMA-based ISAC system, we first develop a beamforming technique for the max-min signal-to-interference-and-noise ratio (SINR) balancing problem. However, the original form is not convex regarding the design parameters. We propose an iterative algorithm that uses a bisection search to address the non-convexity problem and achieve a feasible solution to the original SINR balancing problem. This approach involves solving an equivalent power minimization problem, where we exploit the semidefinite relaxation technique. We also consider a robust design for the power minimization problem by taking into account inevitable imperfect channel state information. The numerical results show that the proposed NOMA-based ISAC performs better than the conventional orthogonal multiple access-based ISAC system in terms of transmit power consumption and balanced SINR while meeting the quality of service requirements regardless of the uncertainty of the associated channel.

C. Li, S. Mohammadzadeh and K. Cumanan are with School of Physics Engineering and Technology, University of York, York, YO10 5DD, U.K. (email: cl2215@york.ac.uk; Saeed.mohammadzadeh@york.ac.uk; kanapathippillai.cumanan@york.ac.uk).

H. Al-Obiedollah is with the Wireless Communications, Department of Electrical Engineering, The Hashemite University, Zarqa, Jordan (email: haithamm@hu.edu.jo).

O. A. Dobre is with the Department of Electrical and Computer Engineering, Memorial University, St. John's NL A1B, Canada (email:odobre@mun.ca).

Index Terms

Integrated Sensing and Communication, Non-Orthogonal Multiple Access, signal-to-interference-and-noise ratio balancing, and power minimization.

I. Introduction

Future wireless communications systems, including sixth-generation (6G) and beyond, are expected to meet unprecedented requirements such as higher spectral and energy efficiency, massive connectivity to support smart cities and homes, and precise sensing capabilities for emerging novel applications [1]. In this context, sensing becomes increasingly important as it plays a key role in providing more information, such as location data from the environment [2]. Therefore, advanced joint system design could integrate communication, sensing, control, and computation are being considered to support smart cities and other new applications of the Internet of Things (IoT) in 6G and beyond [1]. In line with this trend, the idea of an integrated sensing and communication (ISAC) system appears as a critical solution, integrating communication and radar sensing functions on a single platform to serve both communication users and sensing targets. By sharing the same spectrum, ISAC enhances resource efficiency while enabling sensing capabilities that support various IoT applications [1]. In fact, in an effort to smoothly integrate sensing and communication into a single system, ISAC systems are currently shifting toward the use of larger antenna arrays, operation at higher frequency bands, and increased miniaturization.

Another challenge that must be considered is the exponential growth of mobile users, and various IoT devices present a significant challenge to provide massive connectivity in 6G and beyond. However, existing designs from previous generations of wireless technology struggle to meet these stringent requirements. Even if we focus only on communicating users, traditional orthogonal multiple access (OMA) technology struggles to accommodate such a large user due to its limited degree of freedoms (DoFs). To address this, non-orthogonal multiple access (NOMA) has been recommended as a feasible technique, which can transmit superposition coded (SC) signals and adopt successive interference cancellation (SIC) to introduce additional DoFs in the power domain, thereby facilitating non-orthogonal resource sharing among more users [3]. This can enhance DoFs for communication users while allowing the integration of sensing targets [4], [5].

In summary, NOMA provides efficient interference management and flexible resource allocation, which is suitable for integration with ISAC systems. Incorporating NOMA into the foundational ISAC system can effectively support the massive number of users and devices that are anticipated in the next generation of wireless networks. Hence, a NOMA-based ISAC (NOMA-ISAC) system is an ideal communication system where the complementary benefits of each technique are exploited. In addition, this enhances the system's capacity to accommodate a growing number of communication users while supporting sensing capabilities.

A. Prior and Related Works

Preceding the advent of the ISAC systems, substantial research efforts have been made over the past decade to co-exist with various communication and sensing systems. Initially, efforts have been focused on embedding communication information in the radar waveform [1]. When using orthogonal frequency division multiplexing (OFDM), an essential technique in wireless networks, two designs emerged: radar-centric (or sensing-centric) and communication-centric designs by modifying their original waveforms to serve both communication users and sensing targets simultaneously, and some technologies are independent of the underlying systems and signals [6]. The radar-centric design is suitable when high throughput is unnecessary, as communication assumes a secondary role. In contrast, communication-centric design tends to have high throughput to meet the communication requirement. Both designs attempt to exploit the strengths of one waveform to serve sensing targets and communication users and enhance overall functionality.

However, a key limitation is that they tend to optimize one function at the expense of the other, resulting in suboptimal performance. To overcome this challenge, recent advancements have focused on developing a unified waveform that can support sensing and communication functions at the same time, a concept referred to as co-design.

This system that combines sensing and communication was known by a number of names, including radar-communication (RadCom) [7], [8] and joint radar and communication (JRC) [9]. RadCom systems, which exploit similar architectures and carrier frequencies, are effective for simultaneous data transmission and sensing, enabling communication and remote sensing [7], [8], [10]. JRC systems aim to balance radar and communication performance while mitigating interference, with multi-input multi-output (MIMO) integration identified as a key strategy to enhance interference reduction [6], [9], [11], [12]. Building on these works, the ISAC system proposes that

communication and sensing services can use the same frequency band and technological device by designing a shared waveform, thereby enhancing spectrum efficiency and reducing hardware cost [13]. ISAC not only supports communication users but also performs sensing tasks such as positioning and tracking, enhancing applications such as smart cities and vehicle-to-everything (V2X) applications [1]. Furthermore, ISAC supports advanced applications, including advanced positioning and tracking, sensing-aided beam training, and resource allocation [13].

To improve the accuracy of the ISAC, the transmitter is designed to focus the power toward specific areas of interest, thereby achieving accurate target estimation while maintaining reliable service for communication users [13]. Hence, beamforming design has become an effective approach in ISAC systems to meet both communication and sensing requirements [14], [15]. This technology allows the transmitter to direct its energy toward specific communication users or targets, thereby improving signal strength and quality, reducing interference, and maximizing spectral efficiency; the shared spectrum could be considered for beamforming. The use of beamforming in ISAC systems can effectively allocate shared spectrum resources, ensuring robust performance for communication and sensing applications [10].

However, the DoFs become greatly limited as the number of users and targets rises, particularly when their number exceeds the number of antennas, which poses a significant challenge to the ISAC system [14]. Therefore, NOMA has been introduced to provide additional DoFs to support a larger number of communication users and sensing targets.

NOMA is a future-oriented, efficient multiple-access technology due to its advantages in spectral and energy efficiency, fairness, and capacity to support massive connectivity. NOMA allows multiple communication users to share time-frequency resources simultaneously through multiplexing of the power domain, effectively improving the system's DoFs [16]. Specifically, the base station (BS) simultaneously transmits a SC signal to each NOMA receiver. Users with stronger channel conditions first decode the signals for the weaker users and apply SIC to subtract these signals from the SC transmission, then decode their own signals. Meanwhile, users with weaker channel conditions decode only their own signals, treating the signals of other users as interference, allowing them to be allocated more power [17]–[19]. This differentiation allows the system to exploit the varying channel conditions of the users, effectively increasing the DoFs, and the SIC could reduce interference between each user.

Because NOMA provides efficient interference management and flexible resource allocation, it is ideal for integration with the ISAC system, enabling support for more users while effectively

minimizing interference in future networks. Therefore, we aim to develop a NOMA-based ISAC system, referred to as NOMA-ISAC, which combines NOMA and ISAC technologies. In this system, the BS simultaneously sends information to communication users and probing targets, and communication users exploit NOMA to improve both spectral and energy efficiencies. Therefore, the NOMA-ISAC system can effectively utilize limited DoFs to accommodate more communication users and ensure the sensing targets receive sufficient power to perform their functions by sharing the same beamforming and hardware platform with communication services.

Several studies have explored optimizing performance metrics in NOMA-ISAC systems. In [20], the authors propose uplink and downlink models for NOMA-ISAC, where the uplink design facilitates flexible resource allocation between the communication and sensing functions, and the downlink designs aim to reduce interference for inter-communication users and between communication users and sensing targets. The study in [21] solved the problem of minimizing transmit power while satisfying the probability constraints of outages of communication users and the target requirements. Similarly, [22] introduces a resource allocation technique to maximize weighted sum throughput while optimizing sensing power, while [23] proposes strategies to enhance spectral efficiency under performance constraints. Lastly, [24] investigates inter-user interference and suggests a two-stage SIC-based framework to manage interference between communication users and sensing targets.

B. Contributions and Notation

Motivated by the above-mentioned work, we investigate a downlink transmission in a NOMA-ISAC system and solve two resource allocation problems. The first is the max-min SINR balancing problem, where the minimum SINR of the users is maximized to maintain fairness between users. The second is the power minimization problem, where the total transmit power is minimized while satisfying the required quality of services. Specifically, we consider two scenarios for the power minimization problem: one with perfect channel state information (CSI) and the other with imperfect CSI assumption. The key contributions and findings of the paper are outlined as follows:

- In order to maintain user fairness, we formulate a max-min SINR balancing problem for communication users within a total power constraint while guaranteeing sufficient power allocation for the sensing target. In order to address the original problem's non-convexity,

we employ an iterative bisection search, which is exploited to obtain near-optimal solutions, ensuring efficient resource allocation.

- Given the close relationship between the max-min SINR problem and the power minimization problem, where the goal is to minimize the total transmit power while ensuring communication users meet their required SINR threshold and the sensing target receives sufficient power, we consider solving the non-convex power minimization problem through semidefinite relaxation (SDR) techniques under perfect CSI assumption.
- Due to practical limitations, we also formulate a robust power minimization problem to mitigate the impact of channel uncertainties. Under the imperfect CSI, we adopt a worst-case robust optimization framework to show that robust design meets system requirements while guaranteeing that each communication user's and sensing target's service requirements are satisfied.

Overall, the performance of the NOMA-ISAC and OMA-ISAC systems is evaluated and compared based on numerical results. The results of the max-min SINR balancing problem indicate that the NOMA-ISAC system achieves a higher balanced SINR under total transmit power constraints. In the power minimization problem, the simulation results show that the NOMA-ISAC system meets the required SINR thresholds with less power consumption while ensuring sufficient power is allocated to the sensing targets. Additionally, the study also highlights that the NOMA-ISAC system outperforms the OMA-ISAC system in robust design scenarios, indicating its resilience to channel uncertainties.

The remainder of this paper is structured as follows. Section II introduces the system model of a NOMA-ISAC system and defines the constraints for communication users and sensing targets. Section III formulates the max-min SINR balancing problem for the NOMA-ISAC system under the perfect CSI, which is shown to be equivalent to a power minimization problem. Section IV extends the power minimization problem under the imperfect CSI, proposing a robust design to account for channel uncertainties. Section V presents the numerical results of the max-min SINR balancing problem, the power minimization problem under the perfect CSI assumption, and the robust designs under imperfect CSI. Finally, we conclude this paper in Section VI.

Notations: We use lowercase and uppercase boldface letters for vectors and matrices, respectively. $\mathbb{E}\{\cdot\}$ and $\Re\{\cdot\}$ stand for the statistical expectation of random variables and the real part of a complex number, respectively. The symbol $\mathbb{C}$ is used for the complex numbers of n-dimensions and $\mathbb{R}$ for the real numbers. $(\cdot)^H$ and $\mathrm{Tr}(\cdot)$ denote conjugate transpose and the trace of a matrix,

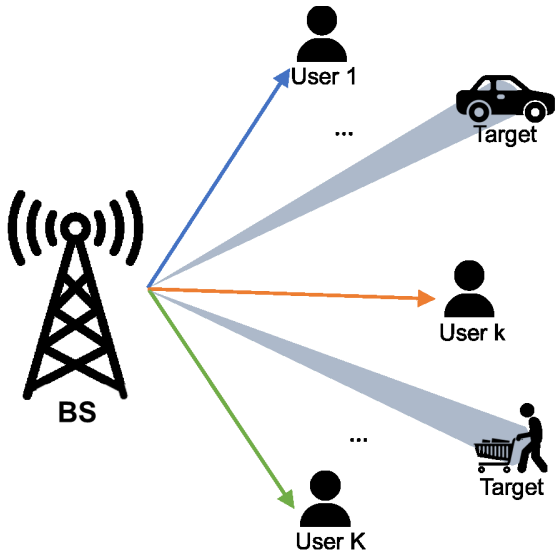

Fig. 1: Illustration of a downlink NOMA-ISAC system.

respectively. The Euclidean norm of a matrix is denoted by $\|\cdot\|_2$. $\mathbf{B} \succeq 0$ indicates that $\mathbf{B}$ is a positive semidefinite matrix.

II. System Model

In this paper, we consider a NOMA-ISAC system, in which a dual functional BS equipped with N antennas communicates with K single-antenna communication users indexed by $\mathcal{K} \in \{1, \cdots, K\}$. Furthermore, the BS serves M sensing targets indexed by $\mathcal{M} \in \{1, \cdots, M\}$ as shown in Fig. 1.

1) Communication Part: The BS in this system utilizes NOMA to send signals to all communication users at the same time using the beamformer $\mathbf{w}_k \in \mathbb{C}^{N\times 1}$ to deliver the symbol s_k, with s_k as the symbol intended for user k. We assumed $\mathbb{E}\{|s_k|^2\} = 1$. Hence, the received signal at user k is excepted as:

$$y_k = \mathbf{h}_k^H \mathbf{w}_k s_k + \sum_{i=1,\, i\neq k}^{K} \mathbf{h}_k^H \mathbf{w}_i s_i + n_k, \tag{1}$$

where $\mathbf{h}_k \in \mathbb{C}^{N\times 1}$ represents the complex channel vector between user k and the BS, n_k stands for zero-mean circularly symmetric additive white Gaussian noise with variance σ_n^2.

Communication users are assumed to decode their messages based on their channel strength following the concept of NOMA, and the channel quality of communication users is ordered as

$||\mathbf{h}_1||_2 \leq ||\mathbf{h}_2||_2 \leq \cdots \leq ||\mathbf{h}_K||_2$. Since NOMA could perform SIC on the communication user receiver to decode the corresponding signal, each user k can detect and remove the signal of the preceding $(k-1)$ users signals successively and treat the signal of the subsequent users $(k+1)$ to the user K as noise [25]. In order to identify user k, the remaining signal at user l is thus represented as follows:

$$y_l^k = \mathbf{h}_l^H \mathbf{w}_k s_k + \sum_{i=k+1}^{K} \mathbf{h}_l^H \mathbf{w}_i s_i + n. \tag{2}$$

To guarantee successful SIC implementation, higher power levels should be assigned to the weaker users; this can be achieved by satisfying the following constraints:

$$\begin{aligned} |\mathbf{h}_k^H \mathbf{w}_1|^2 \geq \cdots \geq |\mathbf{h}_k^H \mathbf{w}_{k-1}|^2 \geq |\mathbf{h}_k^H \mathbf{w}_k|^2 \geq |\mathbf{h}_k^H \mathbf{w}_{k+1}|^2 \geq \\ \cdots \geq |\mathbf{h}_k^H \mathbf{w}_K|^2, \ \forall k \in \mathcal{K}. \end{aligned} \tag{3}$$

Hence, user l decodes the message intended for user k with the following SINR:

$$\text{SINR}_l^k = \frac{|\mathbf{h}_l^H \mathbf{w}_k|^2}{\sum\limits_{i=k+1}^{K} |\mathbf{h}_l^H \mathbf{w}_i|^2 + \sigma^2}. \tag{4}$$

2) Sensing Part: Since sensing targets share the same spectrum with communication users, the ISAC system beamformer can be used to detect targets. The detection signal power $P(\theta_m)$ is directed towards the target's direction when the system is operating in tracking mode, and there is previously detected information about the target [26]. Hence the power $P(\theta_m)$ is given by:

$$P(\theta_m) = \boldsymbol{\alpha}^H(\theta_m) \mathbf{R}_c \boldsymbol{\alpha}(\theta_m), \tag{5}$$

where $\theta_m, \forall m \in \mathcal{M}$ denotes the direction of the target. The corresponding steering vector is expressed as $\boldsymbol{\alpha}(\theta_m) = [1, e^{j\frac{2\pi}{\lambda} d \sin(\theta_m)}, \ldots, e^{j\frac{2\pi}{\lambda} d(N-1)\sin(\theta_m)}]^T$, where λ represent the carrier wavelength, and $d \leq (\lambda/2)$ indicates the antenna spacing, respectively. Moreover, $\mathbf{R}_c$ is the covariance matrix of the transmit signal for sensing user defined as [22]:

$$\mathbf{R}_c = \sum_{k=1}^{K} \mathbf{w}_k \mathbf{w}_k^H. \tag{6}$$

Meanwhile, in order to ensure good sensing quality, the cross-correlation between transmitted signals at a given target location should be as low as possible [26]. Thus, for any two sensing targets directions θ_p and θ_m, the cross-correlation is denoted as $C(\theta_p, \theta_m) =$

$|\boldsymbol{\alpha}^H(\theta_p)\mathbf{R}_c\boldsymbol{\alpha}(\theta_m)|^2, \forall p \neq m \in \mathcal{M}$, while the mean-squared cross-correlation of $\frac{M^2-M}{2}$ pairs of the sensing users is given as:

$$\overline{C} = \frac{2}{M^2 - M} \sum_{p=1}^{M-1} \sum_{m=p+1}^{M} C(\theta_p, \theta_m). \tag{7}$$

III. Max-min SINR Problem for NOMA-ISAC System

In this section, we examine the problem of maximizing the minimum achievable SINR of communication users under a given total power constraint (max-min SINR) while ensuring sufficient power allocation to the sensing targets under the perfect CSI. Since the NOMA technique allows for more flexible management of communication users, it may be more efficient to offer a fair SINR performance across the communication users. Additionally, in the NOMA-ISAC system, the power threshold required for sensing targets must be incorporated into the design. Therefore, the problem is defined as:

$$\max \min_{l \in \{k, k+1, \cdots, K\}} \text{SINR}_l^k \tag{8a}$$

$$\text{s.t.} \sum_{k=1}^{K} \|\mathbf{w}_k\|_2^2 + \sum_{m=1}^{M} P(\theta_m) \leq P_{\text{total}}, \tag{8b}$$

$$P(\theta_m) \geq P_s, \ \forall m \in \mathcal{M}, \tag{8c}$$

$$|P(\theta_p) - P(\theta_m)| \leq P_{\text{diff}}, \ \forall p \neq m \in \mathcal{M}, \tag{8d}$$

$$\overline{C} \leq \xi, \tag{8e}$$

where $\|\mathbf{w}_k\|_2^2$ and $P(\theta_m)$ denote the power of the k^{th} communication user and the sensing target, respectively. The P_{total} represents the total transmit power available at the BS. The constraint (8b) ensures that the total power of the communication users and the detection targets is below the available power threshold. Furthermore, P_s represents the minimum sensing power threshold, and constraint (8c) specifies that the power allocated to each sensing target must be higher than the respective power threshold. Moreover, (8d) ensures that the power difference between two sensing targets remains less than the predefined threshold P_{diff}. Finally, an upper bound of the mean-squared cross-correlation is guaranteed by (8e).

However, the max-min problem is inherently non-convex, and the constraints in (8d) are also non-convex due to the quadratic structure of the covariance matrix, making the optimization problem (8) challenging to solve directly. In order to address this issue, we utilize the bisection

method and introduce a slack variable t, representing the minimum SINR for all communication users, which we maximize. Consequently, (8) can be changed as follows:

$$\begin{aligned} &\max \ \ t \\ &\text{s.t.} \ \ \text{SINR}_l^k \geq t, \ \forall k \in \mathcal{K}, \\ &\qquad (8b) - (8e). \end{aligned} \tag{9}$$

Let t^{opt} represent the optimal solution for (9). If $t \geq t^{\text{opt}}$, (9) becomes infeasible; conversely, if $t \leq t^{\text{opt}}$, (9) is feasible. Therefore, (9) is transformed into a feasible problem that aims to find a set of $\mathbf{w} = \{\mathbf{w}_1, \cdots, \mathbf{w}_K\}$ that satisfies all constraints for a given value t. This reformulation enables the application of a bisection method to solve the problem, which efficiently narrows the feasible range until it converges to the specified threshold, reducing the result value toward the global optimal value. By selecting t through the bisection method, the solution is achieved by solving the following problem:

$$\begin{aligned} &\min_{\mathbf{w}_k \in \mathbb{C}^{N\times 1}} \ \ \sum_{k=1}^{K} \|\mathbf{w}_k\|_2^2 + \sum_{m=1}^{M} P(\theta_m) \\ &\text{s.t.} \ \ \text{SINR}_l^k \geq t, \ \forall k \in \mathcal{K} \\ &\qquad (8c) - (8e). \end{aligned} \tag{10}$$

Here, (10) is equivalent to minimizing total transmit power while ensuring that communication users achieve the desired SINR threshold and the sensing target receives sufficient power. To determine a feasible solution for (10), we introduce the new matrix $\mathbf{W}_k = \mathbf{w}_k \mathbf{w}_k^H$ and $\mathbf{H}_k = \mathbf{h}_k \mathbf{h}_k^H$, and follow the trace rule $\mathbf{w}^H \mathbf{H} \mathbf{w} = \text{Tr}(\mathbf{H}\mathbf{w}\mathbf{w}^H) = \text{Tr}(\mathbf{H}\mathbf{W})$. In addition, we define a matrix $\mathbf{A}_m = \boldsymbol{\alpha}(\theta_m)\boldsymbol{\alpha}^H(\theta_m)$. Next, using the new matrices $\mathbf{W}_k$, $\mathbf{H}_k$ and $\mathbf{A}_m$, we can express the power $P(\theta_m)$ in (5) as:

$$\begin{aligned} P(\theta_m) &= \boldsymbol{\alpha}^H(\theta_m)\mathbf{R}_c\boldsymbol{\alpha}(\theta_m) = \text{Tr}(\mathbf{R}_c\boldsymbol{\alpha}(\theta_m)\boldsymbol{\alpha}^H(\theta_m)) \\ &= \text{Tr}(\mathbf{A}_m\mathbf{R}_c) = \sum_{k=1}^{K} \text{Tr}(\mathbf{A}_m\mathbf{W}_k), \ \forall m \in \mathcal{M}. \end{aligned} \tag{11}$$

Hence, the original problem (10) can be rewritten as follows:

$$\min_{\mathbf{W}\in\mathbb{C}^{N\times N}} \quad \sum_{k=1}^{K} \mathrm{Tr}(\mathbf{W}_k) + \sum_{m=1}^{M}\sum_{k=1}^{K} \mathrm{Tr}(\mathbf{A}_m\mathbf{W}_k) \tag{12a}$$

$$\text{s.t. } \mathrm{Tr}(\mathbf{H}_l\mathbf{W}_k) - \gamma_k^{\min}(\sum_{i=k+1}^{K} \mathrm{Tr}(\mathbf{H}_l\mathbf{W}_i) + \sigma_n^2) \geq 0,$$

$$\forall k \in \mathcal{K},\ l = k, k+1, \cdots, K, \tag{12b}$$

$$\mathbf{W}_k = \mathbf{W}_k^H,\ \mathbf{W}_k \succeq 0, \tag{12c}$$

$$\mathrm{rank}(\mathbf{W}_k) = 1, \tag{12d}$$

$$\sum_{k=1}^{K} \mathrm{Tr}(\mathbf{A}_m\mathbf{W}_k) \geq P_s,\ \forall m \in \mathcal{M}, \tag{12e}$$

$$|\sum_{k=1}^{K} \mathrm{Tr}((\mathbf{A}_p - \mathbf{A}_m)\mathbf{W}_k))| \leq P_{\text{diff}},\ \forall p \neq m \in \mathcal{M}, \tag{12f}$$

$$\overline{C} \leq \xi. \tag{12g}$$

Because of the rank-one constraint (12d), (12) is still non-convex. Hence, we propose to transform the problem (12) into a standard semidefinite programming problem by relaxing this constraint through SDR methods; this reformulation allows the problem to be addressed effectively with convex optimization techniques. Therefore, without the rank-one constraint, (12) can be reformulated as follows:

$$\min_{\mathbf{W}\in\mathbb{C}^{N\times N}} \quad \sum_{k=1}^{K} \mathrm{Tr}(\mathbf{W}_k) + \sum_{m=1}^{M}\sum_{k=1}^{K} \mathrm{Tr}(\mathbf{A}_m\mathbf{W}_k) \tag{13a}$$

$$\text{s.t. (12b), (12c), (12e)} - \text{(12g)}. \tag{13b}$$

If a set of rank-one $\mathbf{W}_k$ is obtained as the solution to (13), it provides the optimal solution to (12). In this, the beamforming vector $\mathbf{w}_k$ can be derived from the rank-one solutions $\mathbf{W}_k$ of $\mathbf{w}_k = \sqrt{e_k}\mathbf{v}_k$, where e_k and $\mathbf{v}_k$ denote the maximum eigenvalue and the corresponding eigenvector, respectively. Based on this approach, we can identify a suitable solution for the equivalent power minimization problem and apply a bisection search to solve the max-min SINR problem. The algorithm to determine the optimal value is shown in Algorithm 1.

IV. Robust Beamforming Design in Power Minimization Problem

In the previous section, it was assumed that the considered NOMA-ISAC system has perfect CSI. However, in practical scenarios, the channel estimation and quantization errors make it

Algorithm 1 Bisection algorithm for solving problem (8)

Input: $t_{\min} = 0$; $t_{\max} = \frac{P_{\text{total}}|\mathbf{h}_1|^2}{\sigma_n^2}$; Minimum tolerance μ

1: Initialize $t = (t_{\min} + t_{\max})/2$;

2: **repeat**

3: Solve the (13) to obtain $\mathbf{w}$

4: **if** (13) is feasible

5: $t_{\min} = t$; $t^{\text{opt}} = t$; $\mathbf{w}^{\text{opt}} = \mathbf{w}$

6: **else**

7: $t_{\max} = t$

8: **end if**

9: **until** $(t_{\max} - t_{\min} \leq \mu)$

Output: Optimal value $\mathbf{w}^{\text{opt}}$, $t^{\text{opt}} = \min\limits_{l \in \{k, \cdots, K\}} \text{SINR}_l^k(\mathbf{w}^{\text{opt}})$

impossible to achieve perfect CSI at the transmitter [27] [28]. To overcome these channel uncertainties under imperfect CSI conditions, we explore the robust beamforming design in the NOMA-ISAC system using a worst-case performance optimization methodology. Specifically, we consider the norm-bounded channel uncertainty in this design as follows:

$$\mathbf{h}_l = \hat{\mathbf{h}}_l + \Delta\hat{\mathbf{h}}_l, \tag{14}$$

where $\hat{\mathbf{h}}_l$ and $\Delta\hat{\mathbf{h}}_l$ represent the estimate of the actual channel vector $\mathbf{h}_l$ and the norm-bounded channel estimation error, respectively. We assume that the worst-case channel estimation error is bounded by the error bound threshold $\epsilon \geq 0$. Therefore, (14) should be allowed by the following constraints:

$$\left\|\Delta\hat{\mathbf{h}}_l\right\|_2 = \left\|\mathbf{h}_l - \hat{\mathbf{h}}_l\right\|_2 \leq \epsilon \;\leftrightarrow\; \Delta\hat{\mathbf{h}}_l^H \mathbf{I} \Delta\hat{\mathbf{h}}_l - \epsilon^2 \leq 0, \tag{15}$$

where $\mathbf{I} \in \mathbb{C}^{N \times N}$ is the identity matrix.

Based on the channel ordering presented in (3) and the norm-bounded channel uncertainty defined in (14), the received signal at user l for detecting user k can be expressed as follows:

$$\begin{aligned} y_l^k = \mathbf{h}_l^H \mathbf{w}_k + \sum_{i=1}^{k-1} \Delta\hat{\mathbf{h}}_l \mathbf{w}_i + \sum_{i=k+1}^{K} \mathbf{h}_l^H \mathbf{w}_i + n_l, \\ \forall k \in \mathcal{K},\ l = k, k+1, \cdots, K, \end{aligned} \tag{16}$$

where the first term represents the desired signal to be detected, while the second term corresponds to the signal from previous user 1 to the user $k-1$, which cannot be fully removed due to imperfect CSI at the receiver. The third term is the interference signals from user $k+1$ to user K. Thus, the corresponding SINR of user k at user l is written as:

$$\text{SINR}_l^k = \frac{\mathbf{h}_l^H \mathbf{w}_k \mathbf{w}_k^H \mathbf{h}_l}{\sum\limits_{i=1}^{k-1} \Delta\hat{\mathbf{h}}_l^H \mathbf{w}_i \mathbf{w}_i^H \Delta\hat{\mathbf{h}}_l + \sum\limits_{i=k+1}^{K} \mathbf{h}_l^H \mathbf{w}_i \mathbf{w}_i^H \mathbf{h}_l + \sigma_n^2}. \tag{17}$$

In the following, we focus on a robust beamforming design that ensures SINR requirement for communication users while sensing targets meet their minimum power threshold. Hence, it can be formulated as follows:

$$\min_{\mathbf{w}_k \in \mathbb{C}^{N\times 1}} \quad \sum_{k=1}^{K} \|\mathbf{w}_k\|_2^2 + \sum_{m=1}^{M} P(\theta_m) \tag{18a}$$

$$\text{s.t.} \quad \min_{\|\Delta\hat{\mathbf{h}}_l\|^2 \le \epsilon} (\text{SINR}_l^k) \ge \gamma_k^{\min}, \ \forall k \in \mathcal{K}, \tag{18b}$$

$$\Delta\hat{\mathbf{h}}_l^H \mathbf{I} \Delta\hat{\mathbf{h}}_l - \epsilon^2 \le 0, \tag{18c}$$

$$(8c) - (8e).$$

To solve (18), we employ a similar reformulation approach as used in (12). This allows us to redefine the problem as follows:

$$\begin{aligned} &\min_{\mathbf{W}\in\mathbb{C}^{N\times N}} \quad \sum_{k=1}^{K} \text{Tr}(\mathbf{W}_k) + \sum_{m=1}^{M}\sum_{k=1}^{K} \text{Tr}(\mathbf{A}_m \mathbf{W}_k) \\ &\text{s.t.} \ \ \nu_{kl}, \ \forall k \in \mathcal{K}, \ l = k, k+1, \cdots, K, \\ &\qquad (18c), \ (12e) - (12g), \end{aligned} \tag{19}$$

where ν_{kl} is given as (20) at the top of the next page. However, due to rank-one constraint (12d) and uncertainty channel conditions, it is not feasible to obtain the optimal robust beamforming directly. Instead, the rank-one constraints (12d) could be relaxed using SDR, as previously demonstrated.

To mitigate the impact of unknown channel uncertainties in (18c), we reformulated it to a linear matrix by applying the S-procedure technique [27] [28]. Accordingly, we incorporate (18c) through the S-procedure to transform (20) as follows:

$$\mathbf{S}_{kl} = \begin{bmatrix} \mathbf{\Phi} - \sum_{i=1}^{k-1} \mathbf{W}_i + \lambda \mathbf{I} & \mathbf{\Phi}^H \hat{\mathbf{h}}_l \\ \hat{\mathbf{h}}_l^H \mathbf{\Phi} & \hat{\mathbf{h}}_l^H \mathbf{\Phi} \hat{\mathbf{h}}_l - \sigma_n^2 - \lambda\epsilon^2 \end{bmatrix} \succeq 0, \tag{21}$$

$$
\begin{aligned}
(18b) &= \min_{\|\Delta\hat{\mathbf{h}}_l\|^2\le\epsilon} (\mathrm{SINR}_l^k) \ge \gamma_k^{\min} \\
&= \frac{(\hat{\mathbf{h}}_l+\Delta\hat{\mathbf{h}}_l)^H\mathbf{W}_k(\hat{\mathbf{h}}_l+\Delta\hat{\mathbf{h}}_l)}{\sum\limits_{i=1}^{k-1}\Delta\hat{\mathbf{h}}_l^H\mathbf{W}_i\Delta\hat{\mathbf{h}}_l+\sum\limits_{i=k+1}^{K}(\hat{\mathbf{h}}_l+\Delta\hat{\mathbf{h}}_l)^H\mathbf{W}_i(\hat{\mathbf{h}}_l+\Delta\hat{\mathbf{h}}_l)+\sigma_n^2} \ge \gamma_k^{\min} \\
&= \Delta\hat{\mathbf{h}}_l^H(\frac{\mathbf{W}_k}{\gamma_k^{\min}}-\sum_{i=k+1}^{K}\mathbf{W}_i-\sum_{i=1}^{k-1}\mathbf{W}_i)\Delta\hat{\mathbf{h}}_l+2\Re\{(\hat{\mathbf{h}}_l^H(\frac{\mathbf{W}_k}{\gamma_k^{\min}}-\sum_{i=k+1}^{K}\mathbf{W}_i))\Delta\hat{\mathbf{h}}_l\} \\
&\quad+\hat{\mathbf{h}}_l^H(\frac{\mathbf{W}_k}{\gamma_k^{\min}}-\sum_{i=k+1}^{K}\mathbf{W}_i)\hat{\mathbf{h}}_l-\sigma_n^2\ge 0 \\
&= \nu_{kl}. \qquad (20)
\end{aligned}
$$

---

where $\mathbf{\Phi}=\frac{\mathbf{W}_k}{\gamma_k^{\min}}-\sum_{i=k+1}^{K}\mathbf{W}_i$, and $\lambda\ge 0$, the proof of $\mathbf{S}_{kl}$ is defined in Appendix A.

Lemma 1: The problem in (18) can be reformulated by relaxing the rank-one constraint and utilizing the S-procedure, leading to the following equivalent representation:

$$
\begin{aligned}
&\min_{\mathbf{W}\in\mathbb{C}^{N\times N}} \sum_{k=1}^{K}\mathrm{Tr}(\mathbf{W}_k)+\sum_{m=1}^{M}\sum_{k=1}^{K}\mathrm{Tr}(\mathbf{A}_m\mathbf{W}_k) \\
&\text{s.t. } \mathbf{W}_k\succeq 0,\ \mathbf{S}_{kl}\succeq 0,\ \forall k\in\mathcal{K},\ l=k,k+1,\cdots,K, \\
&\qquad (12e)-(12g),
\end{aligned} \qquad (22)
$$

where the problem in (22) is feasible, a rank-one optimal solution $\{\mathbf{W}_k^*\}$ is always existent.

Proof: Refer to Appendix B.

For the sensing part, studies [22], [26], and [29] demonstrate that beamforming can be used to express the sensing power, indicating that (12e) to (12g) only rely on beamforming vectors $\mathbf{w}$ when prior information about the sensing target is available. Thus, if beamforming is used to calculate the power requirement of a sensing target, the channel uncertainty will have little impact on the determined power requirement.

Considering the above, we claim that, whether the CSI is perfect or imperfect, the equations (12e) to (12g) can be used to perform the requirement for sensing targets [30]. Furthermore, the beamforming algorithm can robustly and efficiently optimize the transmit parameters to meet the requirements of the target under different channel conditions. This ensures that the sensing target receives sufficient power to operate reliably regardless of the uncertainties in the channel.

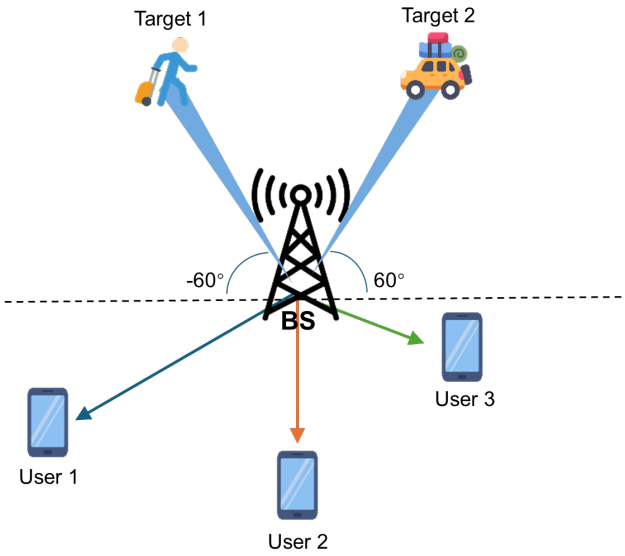

Fig. 2: Simulation of a downlink NOMA-ISAC model.

V. Simulation Results

This section presents simulation results that illustrate the beamforming designs of NOMA in the ISAC system. We consider a NOMA-ISAC system in a single-cell downlink network. The dual-functional BS is equipped with $N = 8$ antennas, serving $K = 3$ communication users and $M = 2$ sensing targets, as shown in Fig. 2. Small-scale fading channels are modeled by Rayleigh fading to represent an isotropic scattering environment. The noise variance for each communication user is assumed to be $\sigma_n^2 = 0.01$, with identical SINR requirements across all users. For the sensing targets, the angles of two sensing targets are $\theta_1 = -60°$ and $\theta_2 = 60°$, with a power differential between them set to $P_{\text{diff}} = 0.001$, and the cross-correlation coefficient specified as $\xi = 10$.

Initially, we analyze the performance of the max-min design for NOMA-ISAC and OMA-ISAC systems under perfect CSI, with the minimum tolerance set to $\mu = 0.02$. Fig. 3 illustrates the performance of the bisection search method by plotting the maximum SINR that communication users achieve the total transmit power, under given the sensing target's power threshold requirement of $P_s = 2$W and $P_s = 3$W, respectively. It is shown that, for a specific transmit power threshold, the NOMA-ISAC system can achieve a higher SINR than the OMA-ISAC system. Additionally, when the sensing threshold is increased, the NOMA-ISAC system still outperforms OMA-ISAC in terms of achievable SINR for communication users. This indicates

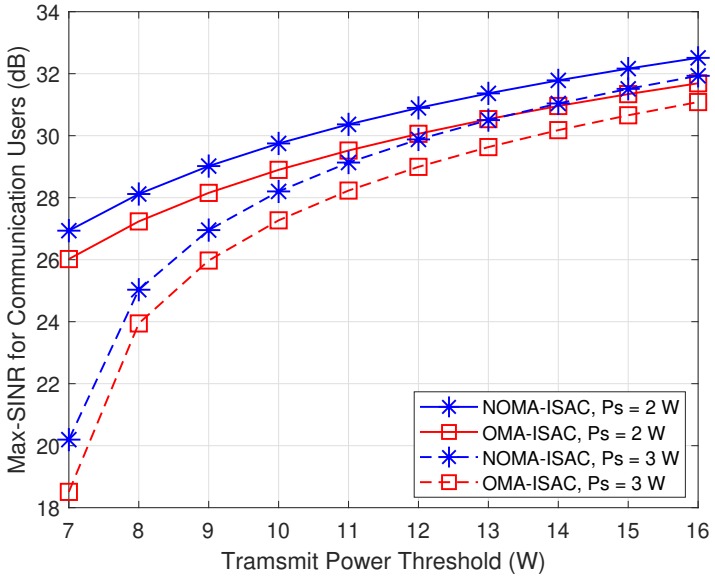

Fig. 3: Achieved max-min SINR versus transmit power in NOMA-ISAC and OMA-ISAC systems with different sensing power thresholds.

that the ability of NOMA-ISAC to multiplex users and dynamically allocate power effectively improves the SINR performance.

Table I presents the achieved SINR for each communication user and allocated power for each sensing target by solving the problem in (8) across five different random channels within the NOMA-ISAC system. Specifically, Table I shows that the max-min design provides the same SINR for all communication users while maintaining uniform power allocations for sensing targets on different channels. This highlights the NOMA-ISAC's capability to allocate power efficiently. By dynamically adjusting power allocations based on channel conditions and quality of service requirements, NOMA-ISAC optimizes resource utilization and enhances system performance in the ISAC scenario.

To verify that the suggested max-min design is optimal, we examine its performance under the same SINR and sensing power thresholds within the same channel by solving the power minimization problem (12). The results are presented in Table II. Table I and Table II show that the max-min and power minimization designs meet the sensing target requirements. By guaranteeing that each communication user reaches the specific SINR threshold, the power-minimization technique produces an ideal solution and validates the optimality of the suggested

TABLE I: Achieved Communication SINR and Sensing Power of the Max-min Design in NOMA-ISAC system in (8).

Channels	P_{total} Threshold (W)	P_s Threshold (watt)	User 1 SINR (dB)	User 2 SINR (dB)	User 3 SINR (dB)	Target 1 Power (W)	Target 2 Power (W)
Channel 1	6	2	24.9986	24.9986	24.9986	2.0000	2.0000
Channel 2	8	2	28.8464	28.8464	28.8464	2.0000	2.0000
Channel 3	10	2	30.2670	30.2670	30.2670	2.0000	2.0000
Channel 4	8	3	26.5256	26.5256	26.5256	3.0000	3.0000
Channel 5	10	3	27.7879	27.7879	27.7879	3.0000	3.0000

TABLE II: Communication SINR and Sensing Power for a given Communication SINR threshold through power minimization in (12).

Channels	SINR Threshold (dB)	P_s Threshold (W)	User 1 SINR (dB)	User 2 SINR (dB)	User 3 SINR (dB)	Target 1 Power (W)	Target 2 Power (W)	P_{total} (W)
Channel 1	24.9986	2	24.9986	24.9986	24.9986	2.0000	2.0000	6
Channel 2	28.8464	2	28.8464	28.8464	28.8464	2.0000	2.0000	8
Channel 3	30.2670	2	30.2670	30.2670	30.2670	2.0000	2.0000	10
Channel 4	26.5256	3	26.5256	26.5256	26.5256	3.0000	3.0000	8
Channel 5	27.7879	3	27.7879	27.7879	27.7879	3.0000	3.0000	10

max-min design.

Next, we evaluate the equivalent proposed power minimization performance based on resource allocation techniques under perfect CSI scenarios in problem (12). Fig. 4 shows the result for this approach given the sensing power thresholds $P_s = 2$W and $P_s = 3$W. In Fig. 4(a), as the SINR threshold increases, the NOMA-ISAC system requires less power to achieve the SINR threshold when compared to the OMA-ISAC system. Fig. 4(b) illustrates the relationship between the total power of sensing for all sensing targets and a given communication SINR threshold. Here, we assume that each sensing target's minimum sensing power threshold is stabilized. As a result, the power allocated to each sensing target remains stable despite the increase in the communication SINR threshold, ensuring that each target's minimum sensing power threshold is always met. Therefore, in the NOMA-ISAC system, communication users can achieve a higher SINR with less transmit power while achieving the minimum power threshold for sensing targets.

Subsequently, as explained in (22), we concentrate on how channel uncertainties affect the total transmit power needed under imperfect CSI. Here, the error bound threshold is set to $\epsilon = 0.05$. The term "Non-robust design" describes a method in which the beamforming vectors are

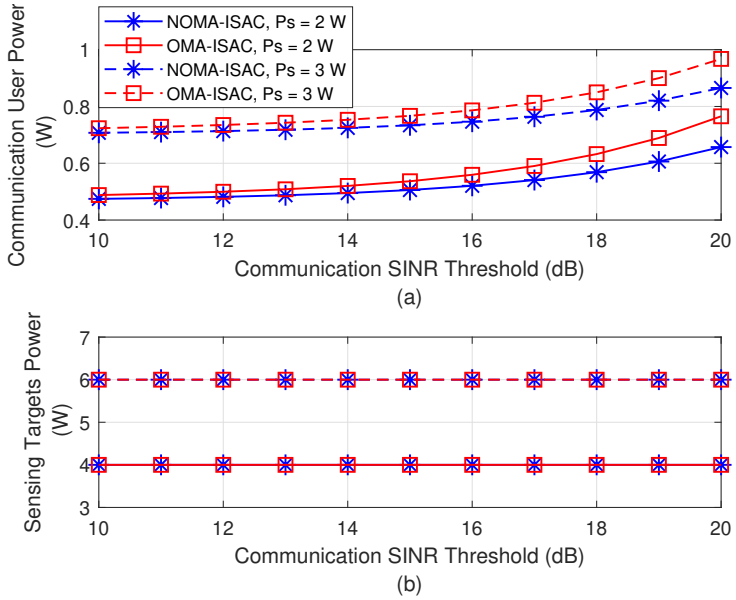

Fig. 4: Achieved power versus SINR in NOMA-ISAC and OMA-ISAC systems.

designed based on imperfect CSI, and the BS has no information on channel uncertainty. Fig. 5 compares the total transmit power required for robust and non-robust NOMA-ISAC systems under varying sensing power and communication SINR thresholds, showing that the robust design demands more power as the SINR threshold increases. To investigate the factors contributing to the increased transmit power required by robust design, we analyze how power allocation is affected as the SINR threshold for communication increases. Specifically, the variations in the total power allocated to communication users and target detection are shown in Fig. 6.

Fig. 6(a) illustrates that the robust design requires more power than the non-robust design, while Fig. 6(b) shows that the sensing power could achieve a minimum power threshold for both robust and non-robust designs. This is due to the assumption that the system has the same sensing power threshold for all SINR thresholds, ensuring that sensing targets meet the minimum required threshold. Thus, despite potential variations in channel conditions and uncertainties in CSI, the robust design employs techniques to ensure that the sensing targets achieve the minimum required power threshold.

Therefore, Fig. 5 and Fig. 6 demonstrate that the robust NOMA design primarily affects the power requirements for the communication part, while the sensing part consistently meets its threshold requirements. Although the non-robust design might require lower transmit power,

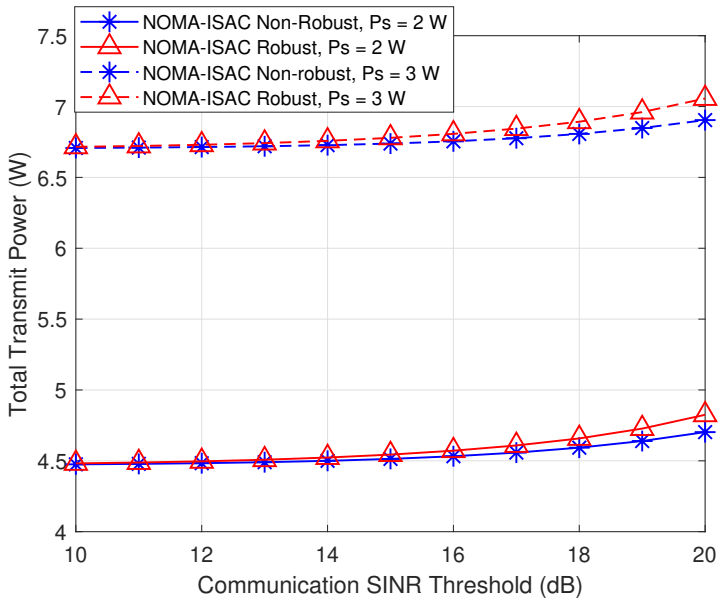

Fig. 5: Achieved total transmit power versus SINR for robust and non-robust design in NOMA-ISAC system.

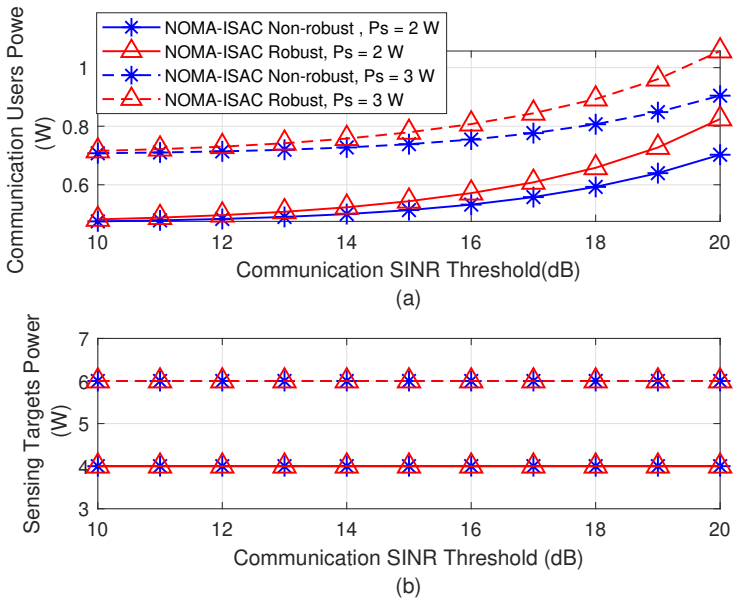

Fig. 6: Achieved power versus SINR for robust and non-robust design in NOMA-ISAC system.

it could struggle to maintain the required SINR threshold under channel uncertainty. This is because, in order to compensate for the effects of the channel, a higher transmit power is needed to achieve the desired SINR threshold under uncertain channel conditions.

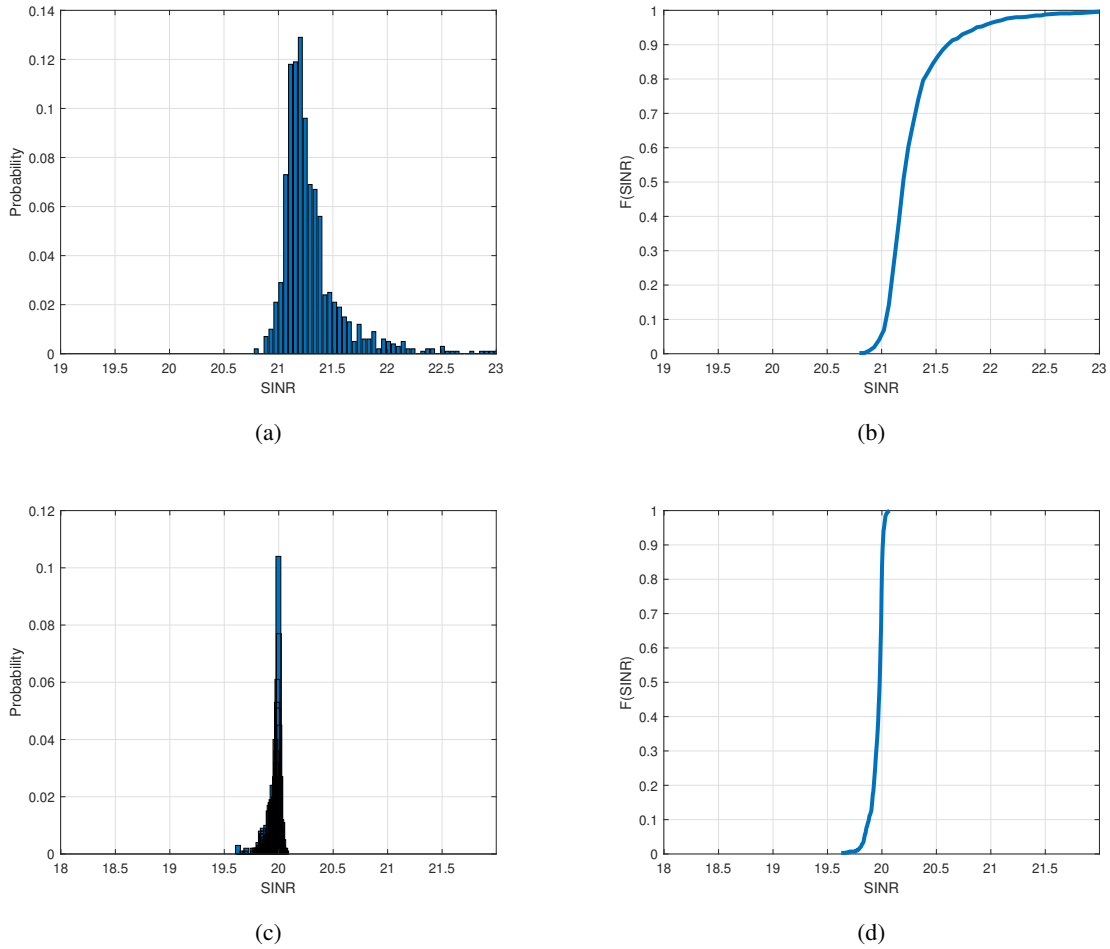

Fig. 7: Comparison PDF and CDF of minimum achieved SINR for robust and non-robust design in NOMA-ISAC system. (a) Robust design PDF. (b) Robust design CDF. (c) Non-robust desing PDF. (D) Non-robust design CDF.

To confirm that the robust NOMA design could always achieve the SINR threshold, we compare the performance of the achieved communication SINR for both robust and non-robust design in the NOMA-ISAC system, which is shown in Fig. 7. In this, the channel error bound is set to $\epsilon = 0.1$, the sensing threshold is $P_s = 2$W, and the SINR threshold is 20 dB for each user. Fig. 7 presents the probability distribution function (PDF) and the cumulative distribution function (CDF) derived from 1,000 random channels. The PDF for the robust design demonstrates that all channels successfully reach the minimum SINR threshold, with the CDF concentrated in a small range, indicating stable performance across channels. On the other hand, the PDF and

CDF plots of the non-robust design fall below the required SINR threshold. This suggests that the non-robust design may struggle to achieve satisfactory SINR levels, particularly in scenarios with channel errors or uncertainties.

Therefore, this robust design demonstrates superior performance in achieving and maintaining desired communication SINR thresholds across uncertain channel conditions, making it more suitable for practical use. By considering uncertainties yielded by imperfect CSI, the robust design significantly enhances system resilience and reliability, leading to consistent satisfaction with SINR requirements for communication users while achieving the requirement of the sensing targets.

VI. Conclusions

In this paper, we proposed two beamforming techniques for an ISAC system based on NOMA, referred to as the NOMA-ISAC system. Specifically, two resource allocation problems for this NOMA-ISAC system were considered: the max-min SINR problem under perfect CSI and minimizing the total transmit power problem under imperfect CSI. To solve the original non-convex problem, we developed an iterative algorithm using SDR techniques for the first problem, which is equivalent to solving the minimized total transmit power problem. For the second robust design problem, non-convex constraints were transformed into a set of linear matrix forms to enhance system performance under channel uncertainties. The simulation results demonstrated the NOMA-ISAC system's performance in achieving balanced SINR and minimizing the required transmit power. These analyses indicated that NOMA-ISAC achieves equivalent SINR thresholds while ensuring the requirement of the sensing targets and outperforms OMA-ISAC under perfect CSI. Furthermore, the results showed that even in the presence of channel uncertainties, the robust design continuously meets SINR requirements, outperforming the non-robust design for communication users.

Appendix A: Proof of (21)

First assume that $f_j(\mathbf{x}), j = 1, 2$ and define:

$$\begin{aligned} f_1(\mathbf{x}) &= \mathbf{x}^H \mathbf{B}_1 \mathbf{x} + 2\Re\{\mathbf{c}_1^H \mathbf{x}\} + q_1 \geq 0, \\ f_2(\mathbf{x}) &= \mathbf{x}^H \mathbf{B}_2 \mathbf{x} + 2\Re\{\mathbf{c}_2^H \mathbf{x}\} + q_2 \geq 0. \end{aligned} \tag{A.1}$$

where $\mathbf{B}_j = \mathbf{B}_j^H \in \mathbb{C}^{N\times N}$, $\mathbf{c}_j \in \mathbb{C}^{N\times 1}$ and $q_j \in \mathbb{R}$. If there exists $\hat{\mathbf{x}}$ to provide $f_1(\hat{\mathbf{x}}) > 0$, then it should have and only have one $\lambda \geq 0$ to implement $f_1(\mathbf{x}) \geq 0 \Rightarrow f_2(\mathbf{x}) \geq 0$, which can written in the following linear matrix inequality:

$$\begin{bmatrix} \mathbf{B}_2 - \lambda \mathbf{B}_1 & \mathbf{c}_2 - \lambda \mathbf{c}_1 \\ \mathbf{c}_2^H - \lambda \mathbf{c}_1^H & q_2 - \lambda q_1 \end{bmatrix} \succeq 0. \tag{A.2}$$

For (20), we assume that $\mathbf{\Phi} = \frac{\mathbf{W}_k}{\gamma_k^{\min}} - \sum_{i=k+1}^{K} \mathbf{W}_i$, hence, (20) can be expressed as follow:

$$\begin{aligned} \nu_{kl} = \Delta\hat{\mathbf{h}}_l^H (\mathbf{\Phi} - \sum_{i=1}^{k-1} \mathbf{W}_i) \Delta\hat{\mathbf{h}}_l + 2\Re\{(\hat{\mathbf{h}}_l^H \mathbf{\Phi}) \Delta\hat{\mathbf{h}}_l\} \\ + \hat{\mathbf{h}}_l^H \mathbf{\Phi} \hat{\mathbf{h}}_l - \sigma_n^2 \geq 0. \end{aligned} \tag{A.3}$$

Meanwhile, (18c) with the express of $\mathbf{B}_1$, $\mathbf{c}_1$, $\mathbf{c}_1^H$ and q_1 is give as follow:

$$f_1(\Delta\hat{\mathbf{h}}_l) = \begin{cases} \mathbf{B}_1 = \mathbf{I}, \\ \mathbf{c}_1 = 0, \\ \mathbf{c}_1^H = 0, \\ q_1 = \epsilon^2. \end{cases} \tag{A.4}$$

Additionally, (A.3) with the form $\mathbf{B}_2$, $\mathbf{c}_2$, $\mathbf{c}_2^H$, and q_2 is given as follow:

$$f_2(\Delta\hat{\mathbf{h}}_l) = \begin{cases} \mathbf{B}_2 = \mathbf{\Phi} - \sum_{i=1}^{k-1} \mathbf{W}_i, \\ \mathbf{c}_2 = \mathbf{\Phi}^H \hat{\mathbf{h}}_l, \\ \mathbf{c}_2^H = \mathbf{\Phi} \hat{\mathbf{h}}_l^H, \\ q_2 = \hat{\mathbf{h}}_l^H \mathbf{\Phi} \hat{\mathbf{h}}_l - \sigma_n^2. \end{cases} \tag{A.5}$$

Replacing (A.4) and (A.5), and replacing into (A.1), the following linear matrix inequality can be written as:

$$\mathbf{S}_{kl} = \begin{bmatrix} \mathbf{\Phi} - \sum_{i=1}^{k-1} \mathbf{W}_i + \lambda \mathbf{I} & \mathbf{\Phi}^H \hat{\mathbf{h}}_l \\ \hat{\mathbf{h}}_l^H \mathbf{\Phi} & \hat{\mathbf{h}}_l^H \mathbf{\Phi} \hat{\mathbf{h}}_l - \sigma_n^2 - \lambda \epsilon^2 \end{bmatrix} \succeq 0. \tag{A.6}$$

APPENDIX B: PROOF OF (22)

The Karush-Kuhn-Tucker (KKT) conditions are examined to prove (22). First, we write the Lagrangian dual function of (22) as follows:

$$\begin{aligned}
&\mathcal{L}(\mathbf{W}, \mathbf{\Lambda}, \mathbf{M}, \mathrm{N}, \mathrm{H}, \mathbf{\Gamma}, \xi) \\
&= \rho_c \sum_{k=1}^{K} \mathrm{Tr}\left(\mathbf{W}_k\right) + \rho_s \sum_{m=1}^{M} \sum_{k=1}^{K} \mathrm{Tr}\left(\mathbf{A}_m \mathbf{W}_k\right) \\
&- \sum_{k=1}^{K} \mathrm{Tr}\left(\mathbf{Y}_k \mathbf{W}_k\right) - \sum_{k=1}^{K-1} \mathrm{Tr}\left(\mathbf{T}_{kl} \mathbf{B}_1\right) \\
&- \sum_{k=1}^{K-1} \mathrm{Tr}[\mathbf{T}_{kl} \mathbf{H}_l^H \mathbf{\Phi} \mathbf{H}_l] - \sum_{k=1}^{K-1} \mathrm{Tr}\left(\mathbf{T}_{kl} \mathbf{B}_2\right) \\
&- \sum_{m=1}^{M} \mathrm{Tr}\left(\mathbf{D}_m \left(\sum_{k=1}^{K} \mathrm{Tr}\left(\mathbf{A}_m \mathbf{W}_k\right) - P_s\right)\right) \\
&+ \sum_{p \neq m}^{M} \mathrm{Tr}\left(\mathbf{F}_{pm}\left(\mathbf{A}_p - \mathbf{A}_m\right) \mathbf{W}_k - P_{\text{diff}}\right) \\
&+ \xi - \left| \alpha^H\left(\theta_p\right) \sum_{k=1}^{K} \mathrm{Tr}\left(\mathbf{W}_k\right) \alpha\left(\theta_m\right) \right|^2,
\end{aligned} \tag{B.1}$$

where $\mathbf{Y}_k$, $\mathbf{T}_{kl}$, $\mathbf{D}_m$ and $\mathbf{F}_{pm}$ are the Lagrangian multipliers associated with the respective constraints, and ξ is a Lagrangian multiplier for the constraint (12g).

The $\mathbf{H}_l$ is defined as $\mathbf{H}_l = [\mathbf{I}\ \mathbf{h}_l]$, and $\mathbf{B}_1$ and $\mathbf{B}_2 =$ are given as:

$$\mathbf{B}_1 = \begin{bmatrix} \lambda \mathbf{I} & \mathbf{0} \\ \mathbf{0} & -\sigma_n^2 - \lambda \epsilon^2 \end{bmatrix}, \mathbf{B}_2 = \begin{bmatrix} -\sum_{i=1}^{k-1} \mathbf{W}_i & \mathbf{0} \\ \mathbf{0} & 0 \end{bmatrix}. \tag{B.2}$$

Hence, the following KKT condition for (B.1) is given as:

$$\begin{aligned}
\frac{\partial \mathcal{L}}{\partial \mathbf{W}_k} &= \mathbf{0}, \\
&= \rho_c \mathbf{I} + \rho_s \sum_{m=1}^{M} \mathbf{A}_m + \mathbf{Y}_k + (\mathbf{H}_l \mathbf{T}_{kl} \mathbf{H}_l) \\
&+ \sum_{m=1}^{M} \mathbf{D}_m + \sum_{p \neq m}^{M} \mathbf{F}_{pm}, \quad \forall k = 1, 2, \ldots, K
\end{aligned} \tag{B.3}$$

and the dual feasibility should be satisfied by the following:

$$\begin{aligned}
&\mathbf{Y}_k \succeq 0,\ \forall k = 1, 2, \ldots, K \\
&\mathbf{D}_m \succeq 0,\ \forall m = 1, 2, \ldots, M \\
&\mathbf{F}_{mk} \succeq 0,\ \forall p \neq m, p, m = 1, 2, \ldots, M, \\
&\qquad \forall k = 1, 2, \ldots, K.
\end{aligned} \tag{B.4}$$

We premultiply (B.3) by $\mathbf{W}_k$, and write the following rank relation:

$$\begin{aligned}
\text{rank}(\mathbf{W}_k) = \text{rank}[&\mathbf{W}_k(\rho_c \mathbf{I} + \rho_s \sum_{m=1}^{M} \mathbf{A}_m + \mathbf{Y}_k \\
&+ (\mathbf{H}_l \mathbf{T}_{kl} \mathbf{H}_l) + \sum_{m=1}^{M} \mathbf{D}_m + \sum_{p \neq m}^{M} \mathbf{F}_{pm})] \\
&= \text{rank}(\mathbf{W}_k \mathbf{H}_l \mathbf{T}_{kl} \mathbf{H}_l) \\
&\leq \min \left\{ \text{rank}(\mathbf{H}_l \mathbf{T}_{kl} \mathbf{H}_l), \text{rank}(\mathbf{W}_k) \right\}.
\end{aligned} \tag{B.5}$$

Based on (B.5), it is required to show that $\text{rank}(\mathbf{H}_l \mathbf{T}_{kl} \mathbf{H}_l) \leq 1$ if we claim that$\text{rank}(\mathbf{W}_k) \leq 1$.

This need to satisfy the complementary slackness, which is given by:

$$\begin{aligned}
&\mathbf{Y}_k \odot \mathbf{W}_k = \mathbf{0}, \quad \forall k = 1, 2, \ldots, K \\
&\mathrm{D}_m \odot \left(\sum_{k=1}^{K} \text{Tr}\left(\mathbf{A}_m \mathbf{W}_k\right) - P_s \right) = \mathbf{0}, \\
&\qquad \forall m = 1, 2, \ldots, M, \quad \forall k = 1, 2, \ldots, K \\
&\mathbf{F}_{pm} \odot \left(\left| \sum_{k=1}^{K} \text{Tr}\left(\left(\mathbf{A}_p - \mathbf{A}_m\right) \mathbf{W}_k \right) \right| - P_{\text{diff}} \right) = \mathbf{0}, \\
&\qquad \forall p \neq m, p, m = 1, 2, \ldots, M.
\end{aligned} \tag{B.6}$$

These conditions together constitute the KKT conditions for the (B.1).

This completes the proof of *Lemma 1*.

REFERENCES

[1] F. Liu, Y. Cui, C. Masouros, J. Xu, T. X. Han, Y. C. Eldar, and S. Buzzi, "Integrated Sensing and Communications: Toward dual-functional wireless networks for 6G and beyond," *IEEE J. Sel. Areas Commun.*, vol. 40, no. 6, pp. 1728–1767, Aug. 2022.

[2] K. B. Letaief, W. Chen, Y. Shi, J. Zhang, and Y.-J. A. Zhang, "The roadmap to 6G: AI empowered wireless networks," *IEEE Commun. Mag.*, vol. 57, no. 8, pp. 84–90, Aug. 2019.

[3] S. R. Islam, N. Avazov, O. A. Dobre, and K.-S. Kwak, "Power-domain non-orthogonal multiple access (NOMA) in 5G systems: Potentials and challenges," *IEEE Commun. Surveys Tuts.*, vol. 19, no. 2, pp. 721–742, Oct. 2016.

[4] J. Choi, "NOMA: Principles and recent results," in *2017 International Symposium on Wireless Communication Systems (ISWCS)*. IEEE, 2017, pp. 349–354.

[5] Y. Liu, S. Zhang, X. Mu, Z. Ding, R. Schober, N. Al-Dhahir, E. Hossain, and X. Shen, "Evolution of NOMA toward next generation multiple access (NGMA) for 6G," *IEEE J. Sel. Areas Commun.*, vol. 40, no. 4, pp. 1037–1071, Apr. 2022.

[6] J. A. Zhang, M. L. Rahman, K. Wu, X. Huang, Y. J. Guo, S. Chen, and J. Yuan, "Enabling joint communication and radar sensing in mobile networks—A survey," *IEEE Commun. Surveys Tuts.*, vol. 24, no. 1, pp. 306–345, Oct. 2021.

[7] C. Sturm and W. Wiesbeck, "Waveform design and signal processing aspects for fusion of wireless communications and radar sensing," *IEEE Proc.*, vol. 99, no. 7, pp. 1236–1259, Jul. 2011.

[8] F. Liu, C. Masouros, A. Li, H. Sun, and L. Hanzo, "MU-MIMO communications with MIMO radar: From co-existence to joint transmission," *IEEE Trans. Wireless Commun.*, vol. 17, no. 4, pp. 2755–2770, Apr. 2018.

[9] F. Liu, C. Masouros, A. P. Petropulu, H. Griffiths, and L. Hanzo, "Joint radar and communication design: Applications, state-of-the-art, and the road ahead," *IEEE Trans. Commun.*, vol. 68, no. 6, pp. 3834–3862, Jun. 2020.

[10] X. Liu, T. Huang, N. Shlezinger, Y. Liu, J. Zhou, and Y. C. Eldar, "Joint transmit beamforming for multiuser MIMO communications and MIMO radar," *IEEE Trans. Sig. Process.*, vol. 68, pp. 3929–3944, Jun. 2020.

[11] F. Dong, W. Wang, Z. Hu, and T. Hui, "Low-complexity beamformer design for joint radar and communications systems," *IEEE Commun. Lett.*, vol. 25, no. 1, pp. 259–263, Jan. 2020.

[12] J. Wang, N. Varshney, C. Gentile, S. Blandino, J. Chuang, and N. Golmie, "Integrated Sensing and Communication: Enabling Techniques, Applications, Tools and Data Sets, Standardization, and Future Directions," *IEEE Internet of Things Journal*, vol. 9, no. 23, pp. 23 416–23 440, Dec. 2022.

[13] Z. Wei, F. Liu, C. Masouros, N. Su, and A. P. Petropulu, "Toward Multi-Functional 6G Wireless Networks: Integrating Sensing, Communication, and Security," *IEEE Commun. Mag.*, vol. 60, no. 4, pp. 65–71, Apr. 2022.

[14] H. Hua, J. Xu, and T. X. Han, "Optimal transmit beamforming for integrated sensing and communication," *IEEE Trans. Veh. Technol.*, Mar. 2023.

[15] A. Bayesteh, J. He, Y. Chen, P. Zhu, J. Ma, A. Shaban, Z. Yu, Y. Zhang, Z. Zhou, and G. Wang, "Integrated sensing and communication (ISAC)—From concept to practice," *Communications of Huawei Research*, pp. 4–25, 2022.

[16] L. Dai, B. Wang, Y. Yuan, S. Han, I. Chih-Lin, and Z. Wang, "Non-orthogonal multiple access for 5G: solutions, challenges, opportunities, and future research trends," *IEEE Commun. Mag.*, vol. 53, no. 9, pp. 74–81, Sept. 2015.

[17] Y. Liu, Z. Qin, M. Elkashlan, Z. Ding, A. Nallanathan, and L. Hanzo, "Nonorthogonal multiple access for 5G and beyond," *IEEE Proc.*, vol. 105, no. 12, pp. 2347–2381, Dec. 2017.

[18] T. Cover, "Broadcast channels," *IEEE Trans. Inf. Theory*, vol. 18, no. 1, pp. 2–14, Jan. 1972.

[19] Q. C. Li, H. Niu, A. T. Papathanassiou, and G. Wu, "5G network capacity: Key elements and technologies," *IEEE Veh. Technol. Mag.*, vol. 9, no. 1, pp. 71–78, Mar. 2014.

[20] X. Mu, Z. Wang, and Y. Liu, "NOMA for integrating sensing and communications towards 6G: A multiple access perspective," *IEEE Wireless Commun.*, Jan. 2023.

[21] X. Huang, G. Zhang, D. Wang, H. Xu, Y. Chen, and R. Li, "Outage constrained transmission design for NOMA-based integrated sensing and communication systems," *Physical Communication*, vol. 63, p. 102292, Apr. 2024.

[22] Z. Wang, Y. Liu, X. Mu, Z. Ding, and O. A. Dobre, "NOMA empowered integrated sensing and communication," *IEEE Commun. Lett.*, vol. 26, no. 3, pp. 677–681, Mar. 2022.

[23] J. Choi, J. Park, N. Lee, and A. Alkhateeb, "Joint and Robust Beamforming Framework for Integrated Sensing and Communication Systems," *arXiv preprint arXiv:2402.09155*, 2024.

[24] C. Ouyang, Y. Liu, and H. Yang, "Revealing the impact of SIC in NOMA-ISAC," *IEEE Wireless Commun. Lett.*, Oct. 2023.

[25] M. F. Hanif, Z. Ding, T. Ratnarajah, and G. K. Karagiannidis, "A minorization-maximization method for optimizing sum rate in the downlink of non-orthogonal multiple access systems," *IEEE Trans. Sig. Process.*, vol. 64, no. 1, pp. 76–88, Jan. 2016.

[26] P. Stoica, J. Li, and Y. Xie, "On probing signal design for MIMO radar," *IEEE Trans. Sig. Process.*, vol. 55, no. 8, pp. 4151–4161, 2007.

[27] F. Alavi, K. Cumanan, Z. Ding, and A. G. Burr, "Robust beamforming techniques for non-orthogonal multiple access systems with bounded channel uncertainties," *IEEE Commun. Lett.*, vol. 21, no. 9, pp. 2033–2036, Sept. 2017.

[28] K. Cumanan, Z. Ding, B. Sharif, G. Y. Tian, and K. K. Leung, "Secrecy rate optimizations for a MIMO secrecy channel with a multiple-antenna eavesdropper," *IEEE Trans. Veh. Technol.*, vol. 63, no. 4, pp. 1678–1690, May. 2014.

[29] R. Li, Z. Xiao, and Y. Zeng, "Beamforming Towards Seamless Sensing Coverage for Cellular Integrated Sensing and Communication," in *2022 IEEE International Conference on Communications Workshops (ICC Workshops)*. IEEE, 2022, pp. 492–497.

[30] Z. Ren, L. Qiu, J. Xu, and D. W. K. Ng, "Robust transmit beamforming for secure integrated sensing and communication," *IEEE Trans. Commun.*, vol. 71, no. 9, pp. 5549–5564, Sept. 2023.